JACS
JOURNAL OF THE AMERICAN CHEMICAL SOCIETY
pubs.acs.org/JACS
Article

Size and Quality Enhancement of 2D Semiconducting Metal–Organic Chalcogenolates by Amine Addition

Watcharaphol Paritmongkol, Tomoaki Sakurada, Woo Seok Lee, Ruomeng Wan, Peter Müller, and William A. Tisdale*

Cite This: J. Am. Chem. Soc. 2021, 143, 20256–20263
Read Online
ACCESS | Metrics & More | Article Recommendations | Supporting Information

ABSTRACT: The use of two-dimensional (2D) materials in next-generation technologies is often limited by small lateral size and/or crystal defects. Here, we introduce a simple chemical strategy to improve the size and overall quality of 2D metal–organic chalcogenolates (MOCs), a new class of hybrid organic–inorganic 2D semiconductors that can exhibit in-plane anisotropy and blue luminescence. By inducing the formation of silver–amine complexes during a solution growth method, we increase the average size of silver phenylselenolate (AgSePh) microcrystals from <5 μm to >1 mm, while simultaneously extending the photoluminescence lifetime and suppressing mid-gap emission. Mechanistic studies using ^{77}Se NMR suggest dual roles for the amine in promoting the formation of a key reactive intermediate and slowing down the final conversion to AgSePh. Finally, we show that amine addition is generalizable to the synthesis of other 2D MOCs, as demonstrated by the growth of single crystals of silver 4-methylphenylselenolate (AgSePhMe), a novel member of the 2D MOC family.

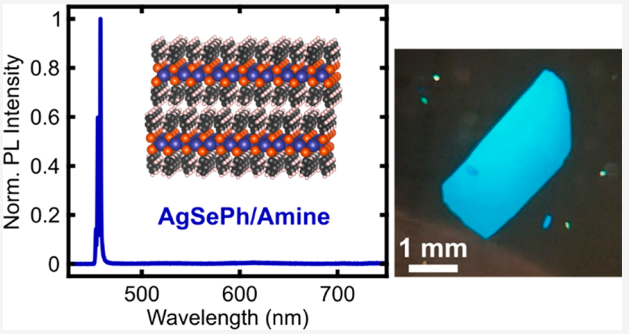

1. INTRODUCTION

Two-dimensional (2D) hybrid organic–inorganic semiconductors exhibit a unique combination of excitonic behavior,[1−4] strong and tunable light–matter interactions,[1−7] and potential applications in optoelectronics.[5,6] An emerging family within this broader class of materials is 2D metal–organic chalcogenolates (MOCs),[8−17] which are synthesized in the form of three-dimensional crystals consisting of 2D layers held together by van der Waals forces. Unlike the more studied ionic 2D lead halide perovskites,[1−6,18] 2D MOCs are distinguished by the covalent interaction between inorganic and organic components. This covalent nature not only makes 2D MOCs stable against both polar and non-polar solvents[16,19] but also allows for unique electronic bandgap tuning by organic modification[20]—a capability not easily achieved in other 2D semiconductors.

Of the 2D MOCs reported so far, silver phenylselenolate (AgSePh)[12,21−27] has received the most attention because of its blue luminescence[12] (Figure 1a) and in-plane anisotropy,[26] which are attractive features for light-emitting applications and light–matter coupling. AgSePh naturally adopts a multi-quantum-well structure consisting of slabs of silver selenide separated by layers of phenyl rings (Figure 1b), leading to a high exciton binding energy of ~400 meV[24,26] and a picosecond photoluminescence (PL) lifetime.[24] Furthermore, AgSePh can be prepared in different forms, depending on the end use need. For example, AgSePh thin films can be prepared by a scalable vapor-phase chemical transformation,[21,25] and microcrystals can be synthesized by a solution-phase hydrothermal synthesis.[22] However, these methods typically yield small AgSePh crystals with average lateral sizes of <5 μm, making fundamental studies and device integration challenging. Additionally, AgSePh samples synthesized by these

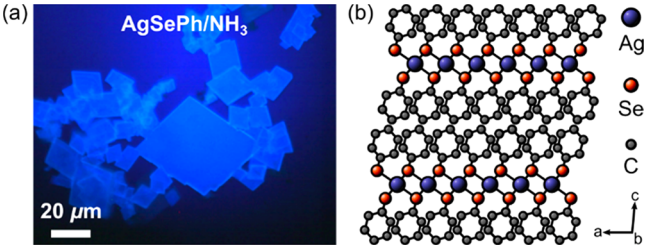

Figure 1. (a) Photoluminescence micrograph of AgSePh microcrystals prepared according to the method reported in this work. (b) Lamellar structure of 2D AgSePh.

Received: August 27, 2021
Published: November 21, 2021

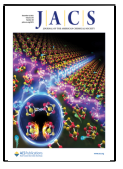

https://doi.org/10.1021/jacs.1c09106
J. Am. Chem. Soc. 2021, 143, 20256–20263

methods show optical and electrical signatures of mid-gap states that may limit AgSePh's optoelectronic performance.[24,27]

In this work, we show that the addition of amines during a solution-phase growth reaction can improve the size and quality of AgSePh crystals. By controlling the amine's alkyl chain length, reagents' concentrations, solvent ratio, and temperature, crystals with sizes ranging from <5 μm to >1 mm, as well as increased PL lifetime and suppression of mid-gap emission, could be synthesized by this simple chemical approach. Reaction kinetics and ^{77}Se nuclear magnetic resonance (NMR) studies were conducted to understand the role of amines during AgSePh growth, and the knowledge gained through this work was used to develop a single-crystal growth method that is applicable to other 2D MOCs, as demonstrated by the synthesis of silver 4-methylphenylselenolate (AgSePhMe), a novel member of the 2D MOC family.

2. RESULTS AND DISCUSSION

2.1. Syntheses of AgSePh Crystals by Amine Addition. AgSePh crystals were synthesized by two different methods: a biphasic hydrothermal reaction (Figure 2a) and an organic single-phase reaction (Figure 2b). For the hydrothermal reaction, a biphasic mixture of diphenyl diselenide (Ph_2Se_2) in toluene and an aqueous solution of silver nitrate ($AgNO_3$) was heated at 180 °C for 1 h to yield AgSePh crystals with average lateral size of ~2 μm (Figure 2a).[22] We found that the size of AgSePh crystals could be increased by the introduction of amines to the reaction mixture. By dissolving $AgNO_3$ in aqueous ammonia (NH_3/H_2O) instead of in pure water (H_2O), the hydrothermal reaction yielded microcrystals with larger sizes of ~20 μm (Figures 1a and 2a). This size improvement was not limited to NH_3/H_2O; larger microcrystals with sizes of ~30 μm and >200 μm could be obtained when aqueous methylamine ($MeNH_2/H_2O$) or aqueous ethylamine ($EtNH_2/H_2O$) were used, respectively (Figure 2a). In all cases, the resulting microcrystals exhibited blue luminescence at 467 nm (Figures 1a and 3a), indicating that amines did not alter the product of the hydrothermal reaction.

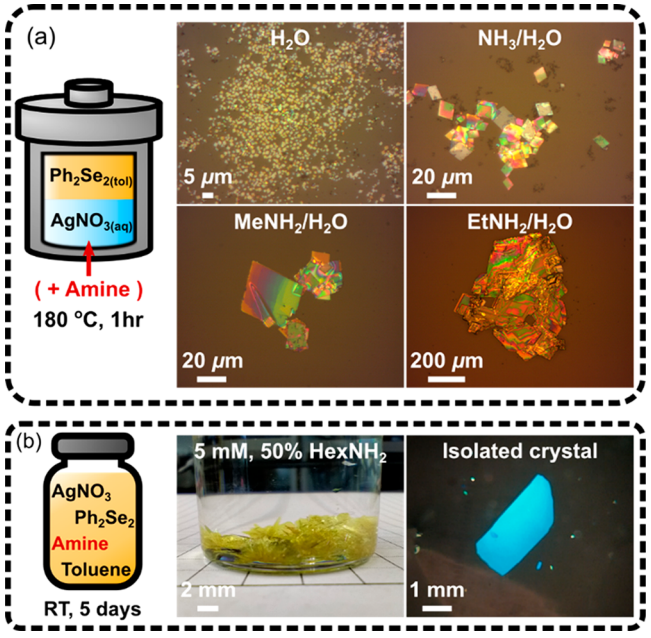

Figure 2. (a) Schematic illustration of a reaction mixture for a hydrothermal reaction (left) and bright-field optical micrographs (right) showing an increase in lateral size upon amine addition. (b) Schematic illustration of a reaction mixture for a single-phase reaction (left), image of the resulting reaction product (middle), and a polarized optical micrograph of an isolated crystal (right).

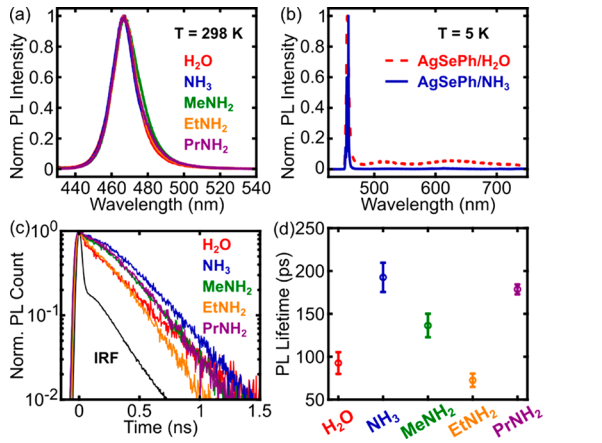

Figure 3. (a) Room-temperature photoluminescence (PL) spectra of AgSePh crystals prepared using water (H_2O), aqueous ammonia (NH_3/H_2O), aqueous methylamine ($MeNH_2/H_2O$), aqueous ethylamine ($EtNH_2/H_2O$), and propylamine ($PrNH_2$). (b) Comparison between PL spectra at 5 K of AgSePh crystals prepared in H_2O and in NH_3/H_2O showing the suppression of broad luminescent features at >500 nm in the latter. (c) Time-resolved PL decays of AgSePh crystals along with the decay due to instrument response function (IRF). (d) Extracted PL lifetimes.

An organic single-phase reaction (Figure 2b) was possible using longer-chain amines, which are liquid at room temperature. In this approach, the reaction was performed in a miscible solution of $AgNO_3$ and Ph_2Se_2 in a combined amine−toluene solution. For instance, equal volumes of a 3 mM solution of $AgNO_3$ in propylamine ($PrNH_2$) and a 3 mM solution of Ph_2Se_2 in toluene were combined to form a 1.5 mM single-phase mixture with 50% v/v $PrNH_2$/toluene. When stored at room temperature for 3−5 days, this solution yielded ~200−500 μm AgSePh crystals (Figure S1) with PL emission centered at 467 nm (Figure 3a). Increasing the reagents' concentrations resulted in the formation of even larger crystals. A 5 mM single-phase mixture with 50% v/v $PrNH_2$ yielded AgSePh crystals with size of >1 μm, and similar results were obtained when amines with longer hydrocarbon chains, such as butylamine ($BuNH_2$) and hexylamine ($HexNH_2$), were used (Figure 2b and S2). While most of these crystals show signs of twinning in polarized light microscopy (Figure S3), isolated millimeter-sized single crystals (Figure 2b and S4) could be obtained through careful searching or cutting. However, these single crystals tended to be too thin for structural refinement by single-crystal X-ray diffraction. Moreover, the crystals could be exfoliated by tape or sonication to obtain multilayered exfoliated flakes (Figure S5) with single-crystal domains as confirmed by electron diffraction (Figure S6).

2.2. Improved Photoluminescence Properties by Amine Addition. In almost all cases, the addition of amines led to an increase in AgSePh PL lifetime. In the presence of NH_3, the PL lifetime doubled from 93 to 193 ps (Figure 3c,d). However, the average PL lifetime decreased to 136 and 73 ps

https://doi.org/10.1021/jacs.1c09106
J. Am. Chem. Soc. 2021, 143, 20256−20263

for crystals made in $MeNH_2/H_2O$ and $EtNH_2/H_2O$, respectively (Figure 3c,d). For these hydrothermally grown AgSePh crystals, the observed PL lifetime trend was correlated with AgSePh reaction kinetics: slower crystal formation at room temperature was observed in an increasing order of $EtNH_2/H_2O$, pure H_2O, $MeNH_2/H_2O$ and NH_3/H_2O, which is the same as the trend of increasing PL lifetime. Slower crystal growth may lead to an increase in PL lifetime by suppressing the formation of crystal defects, which can act as fast nonradiative recombination centers. Slower crystal growth in the presence of amines may be caused by reduced reaction activity of the readily formed silver−amine complexes.[28] On the other hand, the faster kinetics in $EtNH_2/H_2O$ could be explained by the miscibility between $EtNH_2/H_2O$ and toluene, resulting in a single-phase reaction mixture with efficient diffusion of reactive chemical species to the growing crystallites.

An additional benefit of amine-assisted synthesis is the suppression of AgSePh mid-gap luminescence at low temperature. Figures 3b and S7 compare the PL spectra of hydrothermally grown AgSePh crystals with and without NH_3 present during the reaction. At low sample temperature (below ∼150 K), AgSePh crystals prepared in the absence of NH_3 showed broad low-energy PL features spanning 500−700 nm in addition to narrow excitonic emission at ∼460 nm. In contrast, only the narrow excitonic emission was observed for AgSePh crystals grown from NH_3/H_2O. The complete elimination of mid-gap luminescence explains the increased PL lifetime, and suggests that the broad low-energy luminescence band may relate to crystal defects formed during the synthesis and not solely to self-trapped excitons.[29]

However, the possibility of non-luminescent mid-gap states could not be excluded as suggested by temperature-dependent time-resolved photoluminescence (TRPL) spectroscopy (Figure 4a,b). At 200−300 K, the TRPL decay of the NH_3/H_2O sample could be well fitted by a monoexponential function with increasing lifetime upon cooling from 240 ps at 300 K to 720 ps at 200 K (Figure 4c). TRPL behavior underwent a transition to multi-exponential dynamics below ∼150−200 K. From 10 to 150 K, the TRPL decay was well described by a biexponential function (Figure 4b) with a fast decay component ($\tau_{bi,1}$) of ∼210−260 ps, which became more dominating at lower temperature (A_1 in Figure 4d). This transition in temperature-dependent TRPL behavior suggests the presence of an additional excited state in the system such as a non-emissive trapped exciton or a dark exciton, which indirectly influences the dynamics of the radiative excitonic transition at 467 nm.

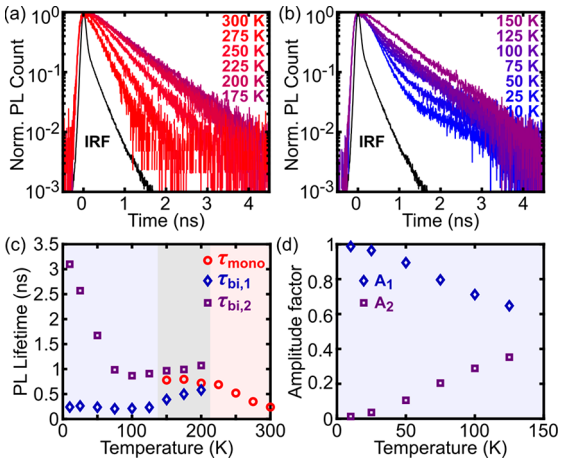

Figure 4. (a, b) Time-resolved PL decays at 10−300 K of AgSePh prepared in NH_3/H_2O along with the decay due to instrument response function (IRF). (c) Extracted temperature-dependent PL lifetimes between 10 and 300 K when fitted with monoexponential (τ_{mono}) and biexponential (τ_{bi}) functions. The shaded gray area between 150 and 200 K denotes the transition between the two different decay models where both fitting models were attempted and compared. (d) Amplitude factors of biexponential fitting between 10 and 125 K.

2.3. Kinetics and Mechanistic Studies. To understand the role of amines in AgSePh synthesis, reaction kinetics studies were conducted (Figure 5a). For simplicity, we focused

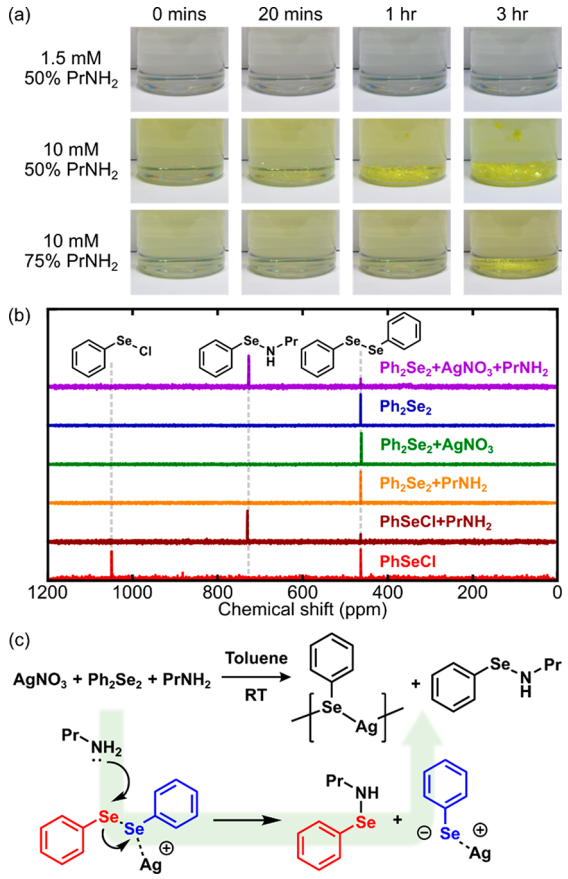

Figure 5. (a) Images of reaction mixtures showing the dependence of crystal formation rate on the solution concentration and the percentage by volume of $PrNH_2$ in the combined $PrNH_2$−toluene solution. (b) ^{77}Se nuclear magnetic resonance spectra of the reaction mixture and its individual components. (c) Proposed mechanism to form AgSePh from $AgNO_3$, Ph_2Se_2, and $PrNH_2$.

our studies on the organic single-phase reaction in $PrNH_2$/toluene to eliminate any effects of the aqueous−organic interface. First, we found that chemical concentrations influenced the kinetics of crystal formation. While a 1.5 mM mixture of $AgNO_3$ and Ph_2Se_2 in 50% v/v $PrNH_2$/toluene did not form crystals until at least 3 days later, increasing the $AgNO_3$ and Ph_2Se_2 concentrations to 10 mM resulted in crystal formation within 20 min. Second, a slower crystal growth rate was observed in a solution mixture with a higher amine content. Compared to the 10 mM solution with 50% v/v $PrNH_2$/toluene whose crystal formation was observed in 20

https://doi.org/10.1021/jacs.1c09106
J. Am. Chem. Soc. 2021, 143, 20256−20263

min, increasing the percentage of $PrNH_2$ to 75% lengthened the crystal formation time to 3 h. These observations suggest that a key role of the amine is to form silver−amine complexes in solution, which subsequently reduce the activity of reactive Ag^+ ions, thereby slowing down crystal growth and allowing for the formation of higher quality crystals.[28] Additionally, the silver−amine complexes may form a lamellar phase and provide a template effect that could lead to the formation of larger crystals as observed in conventional 2D nanocrystals, such as those of II−VI materials.[30−32]

In addition to their role in the formation of silver−amine coordination complexes, amines also react directly with Ph_2Se_2 to form a key reaction intermediate. Using ^{77}Se NMR spectroscopy to study the single-phase reaction between $AgNO_3$ and Ph_2Se_2 in $PrNH_2$/toluene, we observed two peaks in the reaction mixture at 463.15 and 726.69 ppm (Figure 5b, violet). While the former could be assigned to Ph_2Se_2 (Figure 5b, blue), the presence of the latter implied a new Se-containing species in the solution mixture. This Se-containing species was observed only when Ph_2Se_2 was mixed with both $AgNO_3$ and $PrNH_2$ and not in the absence of one of the latter two (Figure 5b, green and orange). We hypothesized that this Se-containing species may be a selenenamide (RSe-NR′R″), as its sulfur analogues, sulfenamides (RS-NR′R″), are known to form when disulfides interact with amines in the presence of Ag^+ ions.[33−36] To confirm our hypothesis, we synthesized a *N*-propylphenylselenenamide (PhSeNHPr) by reacting phenylselenyl chloride (PhSeCl) with $PrNH_2$ (see Section 4.3).[37] The ^{77}Se NMR peak of PhSeNHPr appeared at 729.62 ppm (Figure 5b, brown), agreeing with the previously reported literature[38] and verifying the identity of the second Se-containing species in the reaction mixture.

Determination of the reaction stoichiometry further confirmed the production of selenenamide. We found that a 1:1 ratio of Ph_2Se_2:$AgNO_3$ was needed to obtain 100% formation yield of AgSePh (Figure S8), suggesting that half of the selenium atoms in Ph_2Se_2 were consumed to form AgSePh and the other half were converted into PhSeNHPr. Because Ag^+ ions were needed to see the ^{77}Se NMR peak of PhSeNHPr in the single-phase reaction, we propose that the reaction between Ph_2Se_2 and $PrNH_2$ is facilitated by Ag^+ ions acting as a Lewis acid to weaken the Se−Se bond (Figure 5c). The electrophilic Se−Se bond in Ph_2Se_2 then interacts with nucleophilic $PrNH_2$ to produce PhSeNHPr and a phenylselenolate ion ($PhSe^-$), which later interacts with Ag^+ ions to form AgSePh.

2.4. Growth of MOC Single Crystals. Understanding the role of amines in AgSePh synthesis enabled growth of even higher quality crystals. Mixing a 20 mM solution of $AgNO_3$ in $PrNH_2$ with a 20 mM solution of Ph_2Se_2 in toluene at −20 °C for 4 weeks yielded AgSePh single crystals with size of at least ∼200 μm × ∼200 μm × ∼20 μm (Figure 6a) and sufficient quality for structural refinement by single-crystal X-ray diffraction. We found that the structure of our AgSePh crystals is best described by the monoclinic centrosymmetric space group $P2_1/c$ with a monolayer thickness of 1.4 nm (Figures 6b, S9, and S10, and Table 1). This space group assignment is different from the previous report of a $C2/c$ space group,[39] which could be the result of higher crystal quality with reduced contact twinning or the existence of polymorphs formed in different synthesis conditions, as observed in other MOC materials.[40−42] Compared to the previously reported multi-step method, which involves the use of highly sensitive butyllithium and requires careful preparation,[39] our developed method reduces the synthesis complexity to one step and allows the use of stable reagents.

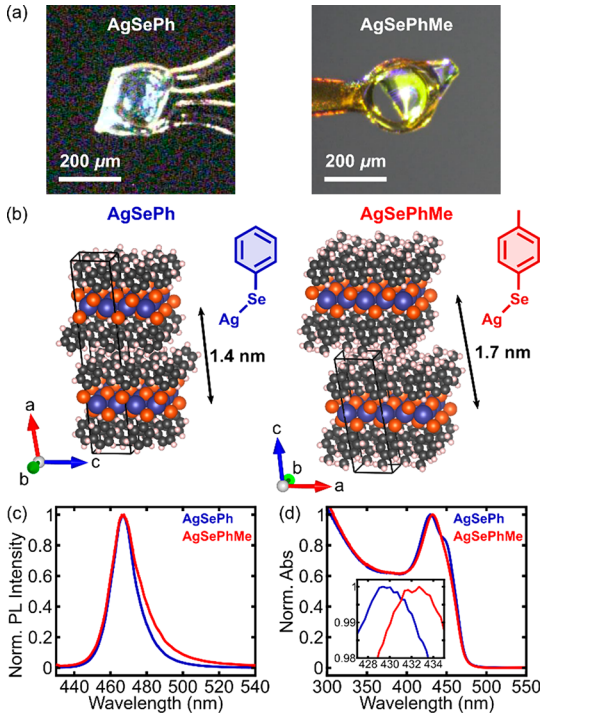

Figure 6. (a) Images of AgSePh and AgSePhMe single crystals used for structural determination. (b) Crystal structures of AgSePh and AgSePhMe. Ag, Se, C, and H atoms are depicted by purple, orange, black, and cream spheres, respectively. (c) Photoluminescence spectra of AgSePh and AgSePhMe. (d) Absorption spectra obtained by diffuse reflectance spectroscopy of AgSePh and AgSePhMe, with an inset showing the zoomed-in view to excitonic absorption peaks.

The amine-assisted crystal growth method is also generalizable to other 2D MOCs. As an example, we grew single crystals of silver 4-methylphenylselenolate (AgSePhMe; Figure 6a)—a new 2D MOC—which crystallized in the monoclinic centrosymmetric space group $P2_1/c$ with a monolayer thickness of 1.7 nm (Figures 6b, S9, and S10, and Table 1). The fact that the structure of AgSePhMe is also best described by the $P2_1/c$ space group further supports our space group assignment of AgSePh above. Compared to AgSePh, AgSePhMe's PL peak appeared at the same wavelength but had a broader FWHM of 19 nm (Figure 6c). However, the excitonic absorption peak shifted from 429 nm in AgSePh to 433 nm in AgSePhMe (Figure 6d), indicating some ability to tune the band gap of 2D MOCs through organic functionalization.[20]

3. CONCLUSION

To summarize, we have shown that size and quality enhancement of AgSePh crystals can be achieved by promoting the formation of silver−amine complexes. Detailed optical characterization by time-resolved and temperature-dependent PL spectroscopy showed that the addition of NH_3 led to a 2-fold increase in PL lifetime and a complete suppression of luminescent mid-gap states. Reaction kinetics studies and mechanistic studies by ^{77}Se NMR spectroscopy suggest dual roles of amines as (1) a coordinating ligand to reduce the reaction activity of Ag^+ ions and (2) a reactant to convert

https://doi.org/10.1021/jacs.1c09106
J. Am. Chem. Soc. 2021, 143, 20256−20263

Table 1. Crystal Data and Structure Refinement for AgSePh and AgSePhMe[a]

	AgSePh	AgSePhMe
identification code	X21004	P21026
empirical formula	$C_{12}H_{10}Ag_2Se_2$	$C_{14}H_{14}Ag_2Se_2$
M_r	527.86	555.91
temperature (K)	100(2)	100(2)
wavelength (Å)	0.71073	0.71073
crystal system	monoclinic	monoclinic
space group	$P2_1/c$	$P2_1/c$
a (Å)	5.8334(5)	17.2752(10)
b (Å)	7.2866(6)	7.2661(4)
c (Å)	29.079(3)	5.7676(3)
α (deg)	90	90
β (deg)	95.5819(16)	99.117
γ (deg)	90	90
V (Å^3)	1230.16(18)	714.82(7)
Z	4	2
calculated density (Mg/m^3)	2.850	2.583
absorption coefficient (mm^{-1})	9.067	7.809
$F(000)$	976	520
crystal size (mm)	0.230 × 0.220 × 0.020	0.230 × 0.215 × 0.010
θ range for data collection (deg)	2.815−31.540	2.803−30.994
index ranges	$-8 \le h \le 8$	$-25 \le h \le 25$
	$-10 \le k \le 10$	$-10 \le k \le 10$
	$-42 \le l \le 42$	$-8 \le l \le 8$
reflections collected	37 922	31 849
independent reflections	4107 [R(int) = 0.0381]	2277 [R(int) = 0.0365]
completeness to θ = 25.242°	99.5%	99.5%
absorption correction	semiempirical from equivalents	semiempirical from equivalents
refinement method	full-matrix least-squares on F^2	full-matrix least-squares on F^2
data/restraints/parameters	4107/32/145	2277/0/84
goodness-of-fit on F^2	1.155	1.147
final R indices [$I > 2\sigma(I)$]	$R1$ = 0.0341	$R1$ = 0.0214
	$wR2$ = 0.1051	$wR2$ = 0.0563
R indices (all data)	$R1$ = 0.0393	$R1$ = 0.0239
	$wR2$ = 0.1090	$wR2$ = 0.0588
largest diff. peak and hole (e·Å^{-3})	1.817 and −2.419	0.534 and −0.978

[a]Additional crystallographic information of AgSePh and AgSePhMe can be found in Section 2 of the Supporting Information.

Ph_2Se_2 into an active intermediate. Based on this knowledge, a new growth method with a single reaction step and stable reactants was developed to grow single crystals of AgSePh. The method was generalizable to other 2D MOCs, such as AgSePhMe, a novel member of this family. The results of this work provide a general strategy for the growth of high-quality 2D MOC materials for further fundamental studies and device integration.

4. EXPERIMENTAL SECTION

4.1. Preparation of Silver Phenylselenolate (AgSePh) Microcrystals by a Hydrothermal Reaction. Microcrystals of AgSePh were prepared by a hydrothermal reaction.[22] A 3 mM solution of silver nitrate ($AgNO_3$; ≥99.0%, Millipore Sigma) was prepared by dissolving 0.0102 g of $AgNO_3$ in 20 mL of either water (H_2O), ammonium hydroxide solution (NH_3/H_2O; ACS reagent, 28.0−30.0% NH_3 basis, Millipore Sigma), methylamine solution ($MeNH_2/H_2O$; 40 wt% in H_2O, Millipore Sigma), or ethylamine solution ($EtNH_2/H_2O$; 68.0 wt% solution in H_2O, Millipore Sigma). In a separate container, a 3 mM solution of diphenyl diselenide (Ph_2Se_2; 97.0+%, TCI America) was prepared by dissolving 0.0187 g of Ph_2Se_2 in 20 mL of toluene. Then, 3 mL of 3 mM $AgNO_3$ solution were transferred into a Teflon lined hydrothermal autoclave reactor (Homend) followed by 3 mL of 3 mM Ph_2Se_2 solution. The hydrothermal reactor was subsequently sealed and placed in an oven at 180 °C. After 1 h, the hydrothermal reactor was removed from the oven and let to cool to room temperature for 1−3 h. Resulting AgSePh microcrystals were then collected by inserting a clean coverslip into a tilted biphasic solution and slowly removing the substrate. The collected microcrystals were washed with isopropanol and dried by compressed nitrogen gas (N_2).

4.2. Preparation of AgSePh Crystals by an Organic Single-Phase Reaction. Crystals of AgSePh were grown by mixing 10 mL of 3 mM solution of $AgNO_3$ in propylamine ($PrNH_2$) with 10 mL of 3 mM solution of Ph_2Se_2 in toluene at room temperature for 3−5 days. $PrNH_2$ can be substituted by other long-chain amines, such as butylamine, pentylamine, and hexylamine, to yield similar results.

4.3. Preparation of *N*-Propylphenylselenenamide. *N*-Propylphenylselenenamide (PhSeNHPr) was synthesized following the previously reported literature.[37,43] $PrNH_2$ (0.035 g, 0.6 mmol) was added to a solution of phenylselenyl chloride (PhSeCl; 0.057 g, 0.3 mmol) in toluene-d_8 (2 mL) in a glovebox. A dark brown solution formed immediately after mixing and then turned into a yellow solution while forming a colorless solid. The resulting solution was filtered and nuclear magnetic resonance (NMR) measurements were carried out without further purification. Diphenyl diselenide (Ph_2Se_2) was added as an NMR standard.

4.4. Preparation of Bis(4-methylphenyl) Diselenide. Bis(4-methylphenyl) diselenide was synthesized following a previously reported procedure.[44,45] First, a crystal of iodine was added to a dispersion of Mg (2.64 g, 110 mmol) in 100 mL of anhydrous tetrahydrofuran (THF) and the mixture was stirred under N_2 atmosphere for 20 min. After the solution became colorless, 4-bromotoluene (3.4 g, 20 mmol) was added at once, and the reaction mixture was heated by a heat gun to initiate the reaction. After that, another portion of 4-bromotoluene (13.7 g, 80 mmol) in THF (50 mL) was added dropwise to a vigorously stirred dispersion. The reaction mixture was further stirred at 50 °C for 1 h before being cooled on ice. Next, elemental selenium (7.9 g, 100 mmol) was added in one portion, and the reaction mixture was allowed to warm to room temperature and stirred for 1 h to yield a yellowish solution. This solution was filtered and poured into 1 M hydrochloric acid (100 mL) to form a biphasic mixture. The organic phase was then extracted with dichloromethane (50 mL × 3) and washed with brine before being dried with sodium sulfate. Subsequently, solvents were evaporated under reduced pressure to obtain a crude product. Purification of this product was performed by column chromatography (hexane) followed by a reprecipitation in dichloromethane and hexane to afford bis(4-methylphenyl) diselenide as orange yellow powder (9.6 g, 56% yield). ^{1}H NMR ($CDCl_3$, 400 MHz) δ 7.50 (d, 4H, J = 8.1 Hz), 7.08 (d, 4H, J = 7.9 Hz), 2.35 (s, 6H).

4.5. Single-Crystal Growth of AgSePh and Silver 4-Methylphenylselenolate (AgSePhMe). Single crystals of AgSePh were obtained by mixing 5 mL of 20 mM solution of $AgNO_3$ in $PrNH_2$ and 5 mL of 20 mM solution of Ph_2Se_2 in toluene at −20 °C for 4 weeks. Single crystals of AgSePhMe were obtained by mixing 5 mL of 15 mM solution of $AgNO_3$ in $PrNH_2$ and 5 mL of 15 mM solution of bis(4-methylphenyl) diselenide in toluene at −20 °C for 4 weeks.

4.6. Nuclear Magnetic Resonance (NMR) Spectroscopy. NMR spectra were recorded with a Bruker Advance 400 MHz spectrometer at 298 K. The spectral data are reported as chemical shift (in ppm). Chemical shifts for ^{77}Se NMR were calibrated against the peak of Ph_2Se_2 (463.15 ppm).

https://doi.org/10.1021/jacs.1c09106
J. Am. Chem. Soc. 2021, 143, 20256−20263

4.7. Steady-State Photoluminescence (PL) Spectroscopy. Steady-state PL measurements were performed on an inverted microscope (Nikon, Ti-U Eclipse) in air. The samples were excited by focusing the output of a 405 nm laser diode (Picoquant, LDHDC-405M, continuous-wave mode) by an objective lens (Nikon, CFI S Plan Fluor ELWD, 40×, 0.6 NA) to <1 μm spot. The polarization of the excitation was controlled to be circularly polarized with a circular polarizer (Thorlabs, CP1R405). After the excitation, the PL was collected in the epi configuration, and passed through a dichroic mirror and a long-pass filter. Then, it was directed into a spectrograph (Princeton Instruments, SP-2500) mounted with a cooled charge-coupled detector (Princeton Instruments, Pixis).

4.8. Time-Resolved PL Spectroscopy. Time-resolved PL measurements were performed using the same microscope setup as steady-state PL spectroscopy with some modifications. The excitation light source was replaced by a frequency-doubled light (405 nm) of the 810 nm output from a femtosecond laser (Coherent Mira HP) operating at 76 MHz. The detector used was a Si avalanche photodiode (Micro Photon Devices) connected to a counting board for time-correlated single-photon counting (PicoQuant, PicoHarp 300). Instrument response function was obtained by detecting the Raman scattering from water appearing at ∼470 nm close to the PL peak position of AgSePh. Extraction of PL lifetime was performed using a publicly available ChiSurf software package developed by Peulen and co-workers.[46]

4.9. Temperature-Dependent PL Spectroscopy. Temperature-dependent experiments were performed by mounting samples on the cold finger of a microscopy cryostat (Janis Research, ST-500) and flowing liquid helium through the cold finger of the cryostat.

4.10. Diffuse Reflectance Spectroscopy. Measurements of diffuse reflectance were performed on a Cary 5000 UV-vis-NIR spectrometer equipped with a PIKE Technologies DiffusIR accessory. Solid samples were prepared by grinding with dry potassium bromide (KBr) to a ∼1 wt% dilution and diffuse reflectance spectra were normalized to a 100% KBr baseline. The obtained diffuse reflectance spectra were converted into absorption spectra by Kubelka–Munk transform:[47]

$$F(R) = \frac{(1 - R)^2}{2R}$$

where $F(R)$ is the Kubelka–Munk function with a value proportional to the sample's absorption coefficient, and R is the relative reflectance of the sample with the 100% KBr baseline.

4.11. Transmission Electron Microscopy (TEM). Samples were prepared by sonicating ∼2 mg of AgSePh or AgSePhMe crystal in ∼2 mL of methanol for 1 h. The crystals were then transferred onto Cu TEM grids via drop-casting. TEM and electron diffraction data were obtained with a Talos Arctica G2 transmission electron microscope operated at an accelerating voltage of 200 kV and an extraction voltage of 4100 kV. Collection of TEM and electron diffraction data were achieved using a Falcon3EC direct electron detector and a Ceta 16M camera, respectively.

4.12. Single-Crystal X-ray Diffraction. Low-temperature diffraction data were collected on Bruker-AXS X8 Kappa Duo diffractometers with IμS micro-sources using Mo Kα radiation (λ = 0.71073 Å), using a Smart APEX2 CCD detector for the structure of AgSePh and a Photon 3 CPAD detector for the structure of AgSePhMe, performing ϕ- and ω-scans. The structures were solved by dual-space methods using SHELXT[48] and refined against F^2 on all data by full-matrix least-squares with SHELXL-2017[49] following established refinement strategies.[50] All non-hydrogen atoms were refined anisotropically. All hydrogen atoms were included into the model at geometrically calculated positions and refined using a riding model. The isotropic displacement parameters of all hydrogen atoms were fixed to 1.2 times the U-value of the atoms they are linked to (1.5 times for the methyl group). Details of the data quality and a summary of the residual values of the refinements are listed in Table 1. Additional crystallographic information—atomic coordinates, isotropic and anisotropic displacement parameters, bond lengths, and bond angles—can be found in Section 2 of the Supporting Information.

Powder X-ray Diffraction (PXRD). PXRD data were collected using a PANalytical Empyrean X-ray diffractometer (Cu Kα radiation, λ = 1.54184 Å). The incident beam path optics included a 1/8° divergence slit, a 10 mm mask, Bragg–Brentano HD optics, a 0.02 rad soller slit, and a 1/4° anti-scatter slit with an illuminated length of 6 mm. The diffracted beam optics included a 0.02 rad soller slit and a PIXcel 1D detector. The angular step in 2θ was 0.013°.

■ ASSOCIATED CONTENT

Supporting Information

The Supporting Information is available free of charge at https://pubs.acs.org/doi/10.1021/jacs.1c09106.

Supplementary Figures S1–S10 and Tables S1–S8, and additional crystallographic information on AgSePh and AgSePhMe (PDF)

Accession Codes

CCDC 2096771 and 2096772 contain the supplementary crystallographic data for this paper. These data can be obtained free of charge via www.ccdc.cam.ac.uk/data_request/cif, or by emailing data_request@ccdc.cam.ac.uk, or by contacting The Cambridge Crystallographic Data Centre, 12 Union Road, Cambridge CB2 1EZ, UK; fax: +44 1223 336033.

■ AUTHOR INFORMATION

Corresponding Author

William A. Tisdale – *Department of Chemical Engineering, Massachusetts Institute of Technology, Cambridge, Massachusetts 02139, United States;* orcid.org/0000-0002-6615-5342; Email: tisdale@mit.edu

Authors

Watcharaphol Paritmongkol – *Department of Chemistry and Department of Chemical Engineering, Massachusetts Institute of Technology, Cambridge, Massachusetts 02139, United States;* orcid.org/0000-0003-1638-6828

Tomoaki Sakurada – *Department of Chemical Engineering, Massachusetts Institute of Technology, Cambridge, Massachusetts 02139, United States*

Woo Seok Lee – *Department of Chemical Engineering and Department of Materials Science and Engineering, Massachusetts Institute of Technology, Cambridge, Massachusetts 02139, United States*

Ruomeng Wan – *Department of Chemistry and Department of Chemical Engineering, Massachusetts Institute of Technology, Cambridge, Massachusetts 02139, United States*

Peter Müller – *Department of Chemistry, Massachusetts Institute of Technology, Cambridge, Massachusetts 02139, United States;* orcid.org/0000-0001-6530-3852

Complete contact information is available at: https://pubs.acs.org/10.1021/jacs.1c09106

Notes

The authors declare no competing financial interest.

■ ACKNOWLEDGMENTS

This work was supported by the U.S. Army Research Office under Award Number W911NF-20-1-0200. This work made use of the MRSEC Shared Experimental Facilities at MIT, supported by the National Science Foundation under award number DMR-08-19762. TEM and electron diffraction data were collected at the Automated Cryogenic Electron

Microscopy Facility in MIT.nano on a Talos Arctica microscope, which was a gift from the Arnold and Mabel Beckman Foundation. We thank Dr. Edward Brignole and Prof. Mircea Dincă for support and assistance with TEM and electron diffraction data collection. T.S. was supported by AGC Inc. (former Asahi Glass Co., Ltd.). W.S.L. was partially supported by the Seoul Broadcasting System Foundation Overseas Doctoral Program Scholarship.

REFERENCES

(1) Mauck, C. M.; Tisdale, W. A. Excitons in 2D Organic−Inorganic Halide Perovskites. *Trends Chem.* **2019**, *1* (4), 380−393.
(2) Blancon, J.-C.; Even, J.; Stoumpos, C. C.; Kanatzidis, M. G.; Mohite, A. D. Semiconductor Physics of Organic−Inorganic 2D Halide Perovskites. *Nat. Nanotechnol.* **2020**, *15* (12), 969−985.
(3) Katan, C.; Mercier, N.; Even, J. Quantum and Dielectric Confinement Effects in Lower-Dimensional Hybrid Perovskite Semiconductors. *Chem. Rev.* **2019**, *119* (5), 3140−3192.
(4) Smith, M. D.; Connor, B. A.; Karunadasa, H. I. Tuning the Luminescence of Layered Halide Perovskites. *Chem. Rev.* **2019**, *119* (5), 3104−3139.
(5) Zhang, F.; Lu, H.; Tong, J.; Berry, J. J.; Beard, M. C.; Zhu, K. Advances in Two-Dimensional Organic−Inorganic Hybrid Perovskites. *Energy Environ. Sci.* **2020**, *13* (4), 1154−1186.
(6) Li, X.; Hoffman, J. M.; Kanatzidis, M. G. The 2D Halide Perovskite Rulebook: How the Spacer Influences Everything from the Structure to Optoelectronic Device Efficiency. *Chem. Rev.* **2021**, *121* (4), 2230−2291.
(7) Dyksik, M.; Wang, S.; Paritmongkol, W.; Maude, D. K.; Tisdale, W. A.; Baranowski, M.; Plochocka, P. Tuning the Excitonic Properties of the 2D $(PEA)_2(MA)_{n-1}Pb_nI_{3n+1}$ Perovskite Family via Quantum Confinement. *J. Phys. Chem. Lett.* **2021**, *12* (6), 1638−1643.
(8) Lavenn, C.; Guillou, N.; Monge, M.; Podbevšek, D.; Ledoux, G.; Fateeva, A.; Demessence, A. Shedding Light on an Ultra-Bright Photoluminescent Lamellar Gold Thiolate Coordination Polymer $[Au(p\text{-}SPhCO_2Me)]_n$. *Chem. Commun.* **2016**, *52* (58), 9063−9066.
(9) Veselska, O.; Podbevšek, D.; Ledoux, G.; Fateeva, A.; Demessence, A. Intrinsic Triple-Emitting 2D Copper Thiolate Coordination Polymer as a Ratiometric Thermometer Working over 400 K Range. *Chem. Commun.* **2017**, *53* (90), 12225−12228.
(10) Veselska, O.; Okhrimenko, L.; Guillou, N.; Podbevšek, D.; Ledoux, G.; Dujardin, C.; Monge, M.; Chevrier, D. M.; Yang, R.; Zhang, P.; et al. An Intrinsic Dual-Emitting Gold Thiolate Coordination Polymer, $[Au(+I)(p\text{-}SPhCO_2H)]_n$, for Ratiometric Temperature Sensing. *J. Mater. Chem. C* **2017**, *5* (38), 9843−9848.
(11) Veselska, O.; Cai, L.; Podbevšek, D.; Ledoux, G.; Guillou, N.; Pilet, G.; Fateeva, A.; Demessence, A. Structural Diversity of Coordination Polymers Based on a Heterotopic Ligand: Cu(II)-Carboxylate vs Cu(I)-Thiolate. *Inorg. Chem.* **2018**, *57* (5), 2736−2743.
(12) Schriber, E. A.; Popple, D. C.; Yeung, M.; Brady, M. A.; Corlett, S. A.; Hohman, J. N. Mithrene Is a Self-Assembling Robustly Blue Luminescent Metal−Organic Chalcogenolate Assembly for 2D Optoelectronic Applications. *ACS Appl. Nano Mater.* **2018**, *1* (7), 3498−3508.
(13) Low, K.-H.; Roy, V. A. L.; Chui, S. S.-Y.; Chan, S. L.-F.; Che, C.-M. Highly Conducting Two-Dimensional Copper(I) 4-Hydroxythiophenolate Network. *Chem. Commun.* **2010**, *46* (39), 7328.
(14) Su, W.; Hong, M.; Weng, J.; Cao, R.; Lu, S. A Semiconducting Lamella Polymer $[\{Ag(C_5H_4NS)\}_n]$ with a Graphite-Like Array of Silver(I) Ions and Its Analogue with a Layered Structure. *Angew. Chem., Int. Ed.* **2000**, *39* (16), 2911−2914.
(15) Hu, L.; de la Rama, L. P.; Efremov, M. Y.; Anahory, Y.; Schiettekatte, F.; Allen, L. H. Synthesis and Characterization of Single-Layer Silver−Decanethiolate Lamellar Crystals. *J. Am. Chem. Soc.* **2011**, *133* (12), 4367−4376.
(16) Wang, Q.; Dong, S.-L.; Tao, D.-D.; Li, Z.; Jiang, Y.-B. Ag(I)-Thiolate Coordination Polymers: Synthesis, Structures and Applications as Emerging Sensory Ensembles. *Coord. Chem. Rev.* **2021**, *432*, 213717.
(17) Wu, Z.; Yao, Q.; Liu, Z.; Xu, H.; Guo, P.; Liu, L.; Han, Y.; Zhang, K.; Lu, Z.; Li, X.; et al. Multiscale Assembly of $[AgS_4]$ Tetrahedrons into Hierarchical Ag−S Networks for Robust Photonic Water. *Adv. Mater.* **2021**, *33* (8), 2006459.
(18) Paritmongkol, W.; Dahod, N. S.; Stollmann, A.; Mao, N.; Settens, C.; Zheng, S.-L.; Tisdale, W. A. Synthetic Variation and Structural Trends in Layered Two-Dimensional Alkylammonium Lead Halide Perovskites. *Chem. Mater.* **2019**, *31* (15), 5592−5607.
(19) Veselska, O.; Demessence, A. d^{10} Coinage Metal Organic Chalcogenolates: From Oligomers to Coordination Polymers. *Coord. Chem. Rev.* **2018**, *355*, 240−270.
(20) Li, Y.; Jiang, X.; Fu, Z.; Huang, Q.; Wang, G.-E.; Deng, W.-H.; Wang, C.; Li, Z.; Yin, W.; Chen, B.; et al. Coordination Assembly of 2D Ordered Organic Metal Chalcogenides with Widely Tunable Electronic Band Gaps. *Nat. Commun.* **2020**, *11* (1), 261.
(21) Trang, B.; Yeung, M.; Popple, D. C.; Schriber, E. A.; Brady, M. A.; Kuykendall, T. R.; Hohman, J. N. Tarnishing Silver Metal into Mithrene. *J. Am. Chem. Soc.* **2018**, *140* (42), 13892−13903.
(22) Popple, D. C.; Schriber, E. A.; Yeung, M.; Hohman, J. N. Competing Roles of Crystallization and Degradation of a Metal−Organic Chalcogenolate Assembly under Biphasic Solvothermal Conditions. *Langmuir* **2018**, *34* (47), 14265−14273.
(23) Huang, Q.-Q.; Li, Y.-Z.; Zheng, Z.; Jiang, X.-M.; Sun, S.-S.; Jiang, H.-J.; Deng, W.-H.; Wang, G.-E.; Zhai, T.-Y.; Li, M.-D.; et al. Single-Component MLCT-Active Photodetecting Material Based on a Two-Dimensional Coordination Polymer. *CCS Chem.* **2020**, *2* (1), 655−662.
(24) Yao, K.; Collins, M. S.; Nell, K. M.; Barnard, E. S.; Borys, N. J.; Kuykendall, T.; Hohman, J. N.; Schuck, P. J. Strongly Quantum-Confined Blue-Emitting Excitons in Chemically Configurable Multiquantum Wells. *ACS Nano* **2021**, *15* (3), 4085−4092.
(25) Maserati, L.; Pecorario, S.; Prato, M.; Caironi, M. Understanding the Synthetic Pathway to Large-Area, High-Quality $[AgSePh]_\infty$ Nanocrystal Films. *J. Phys. Chem. C* **2020**, *124* (41), 22845−22852.
(26) Maserati, L.; Refaely-Abramson, S.; Kastl, C.; Chen, C. T.; Borys, N. J.; Eisler, C. N.; Collins, M. S.; Smidt, T. E.; Barnard, E. S.; Strasbourg, M.; et al. Anisotropic 2D Excitons Unveiled in Organic−Inorganic Quantum Wells. *Mater. Horiz.* **2021**, *8* (1), 197−208.
(27) Maserati, L.; Prato, M.; Pecorario, S.; Passarella, B.; Perinot, A.; Thomas, A. A.; Melloni, F.; Natali, D.; Caironi, M. Photo-Electrical Properties of 2D Quantum Confined Metal−Organic Chalcogenide Nanocrystal Films. *Nanoscale* **2021**, *13* (1), 233−241.
(28) Schmidbaur, H.; Schier, A. Argentophilic Interactions. *Angew. Chem., Int. Ed.* **2015**, *54* (3), 746−784.
(29) Paritmongkol, W.; Powers, E. R.; Dahod, N. S.; Tisdale, W. A. Two Origins of Broadband Emission in Multilayered 2D Lead Iodide Perovskites. *J. Phys. Chem. Lett.* **2020**, *11* (20), 8565−8572.
(30) Nasilowski, M.; Mahler, B.; Lhuillier, E.; Ithurria, S.; Dubertret, B. Two-Dimensional Colloidal Nanocrystals. *Chem. Rev.* **2016**, *116* (18), 10934−10982.
(31) Wang, Y.; Zhou, Y.; Zhang, Y.; Buhro, W. E. Magic-Size II−VI Nanoclusters as Synthons for Flat Colloidal Nanocrystals. *Inorg. Chem.* **2015**, *54* (3), 1165−1177.
(32) Liu, Y.-H.; Wang, F.; Wang, Y.; Gibbons, P. C.; Buhro, W. E. Lamellar Assembly of Cadmium Selenide Nanoclusters into Quantum Belts. *J. Am. Chem. Soc.* **2011**, *133* (42), 17005−17013.
(33) Bentley, M. D.; Douglass, I. B.; Lacadie, J. A.; Weaver, D. C.; Davis, F. A.; Eitelman, S. J. A New One-Step Synthesis of Sulphenamides from Alkyl and Aryl Disulphides. *J. Chem. Soc. D* **1971**, No. 24, 1625−1626.
(34) Davis, F. A.; Friedman, A. J.; Kluger, E. W.; Skibo, E. B.; Fretz, E. R.; Milicia, A. P.; LeMasters, W. C.; Bentley, M. D.; Lacadie, J. A.; Douglass, I. B. Chemistry of the Sulfur-Nitrogen Bond. 12. Metal-Assisted Synthesis of Sulfenamide Derivatives from Aliphatic and Aromatic Disulfides. *J. Org. Chem.* **1977**, *42* (6), 967−972.

https://doi.org/10.1021/jacs.1c09106
J. Am. Chem. Soc. 2021, 143, 20256−20263

(35) Craine, L.; Raban, M. The Chemistry of Sulfenamides. *Chem. Rev.* **1989**, *89* (4), 689−712.
(36) Illyés, T.-Z.; Molnár-Gábor, D.; Szilágyi, L. Novel Approaches to the Syntheses of N-Substituted S-Glycosyl-Sulfenamides. *Carbohydr. Res.* **2004**, *339* (8), 1561−1564.
(37) Paulmier, C. N,N-Diethylbenzeneselenenamide.*Encyclopedia of Reagents for Organic Synthesis*; John Wiley & Sons, Ltd: Chichester, UK, 2001; Vol. 2, pp 2−4. DOI: 10.1002/047084289X.rd177.
(38) Paulmier, C.; Lerouge, P.; Outurquin, F.; Chapelle, S.; Granger, P. ^{1}H, ^{13}C, ^{15}N, ^{17}O and ^{77}Se NMR of Selenenamides. *Magn. Reson. Chem.* **1987**, *25* (11), 955−959.
(39) Cuthbert, H. L.; Wallbank, A. I.; Taylor, N. J.; Corrigan, J. F. Synthesis and Structural Characterization of $[Cu_{20}Se_4(\mu_3\text{-}SePh)_{12}(PPh_3)_6]$ and $[Ag(SePh)]_\infty$. *Z. Anorg. Allg. Chem.* **2002**, *628* (11), 2483−2488.
(40) Lavenn, C.; Okhrimenko, L.; Guillou, N.; Monge, M.; Ledoux, G.; Dujardin, C.; Chiriac, R.; Fateeva, A.; Demessence, A. A Luminescent Double Helical Gold(I)−Thiophenolate Coordination Polymer Obtained by Hydrothermal Synthesis or by Thermal Solid-State Amorphous-to-Crystalline Isomerization. *J. Mater. Chem. C* **2015**, *3* (16), 4115−4125.
(41) Wang, R.-F.; Zhang, W.-G.; Fan, J.; Wang, S.-L. Crystal Structure of Tris(Triphenylphosphine)Bis(μ-Phenyl-Selenolato)-Disilver(I), $Ag_2[P(C_6H_5)_3]_3(C_6H_5Se)_2$. *Z. Kristallogr. - New Cryst. Struct.* **2005**, *220* (1−4), 58−60.
(42) Su, W.; Hong, M.; Weng, J.; Liang, Y.; Zhao, Y.; Cao, R.; Zhou, Z.; Chan, A. S. C. Tunable Polymerization of Silver Complexes with Organosulfur Ligand: Counterions Effect, Solvent- and Temperature-Dependence in the Formation of Silver(I)-Thiolate(and/or Thione) Complexes. *Inorg. Chim. Acta* **2002**, *331* (1), 8−15.
(43) Hiroi, K.; Sato, S. Asymmetric Synthesis with Organo-Selenium Compounds: A Facile Entry to Optically Active 4-Substituted 2-Cyclohexenones by Asymmetric Selenenylation of Ketones with Chiral Selenenamides. *Synthesis* **1985**, *1985* (6/7), 635−638.
(44) Wang, X.; Zhong, Y.; Mo, Z.; Wu, S.; Xu, Y.; Tang, H.; Pan, Y. Synthesis of Seleno Oxindoles via Electrochemical Cyclization of N-arylacrylamides with Diorganyl Diselenides. *Adv. Synth. Catal.* **2021**, *363* (1), 208−214.
(45) Reich, H. J.; Renga, J. M.; Reich, I. L. Organoselenium Chemistry. Conversion of Ketones to Enones by Selenoxide Syn Elimination. *J. Am. Chem. Soc.* **1975**, *97* (19), 5434−5447.
(46) Peulen, T.-O.; Opanasyuk, O.; Seidel, C. A. M. Combining Graphical and Analytical Methods with Molecular Simulations To Analyze Time-Resolved FRET Measurements of Labeled Macromolecules Accurately. *J. Phys. Chem. B* **2017**, *121* (35), 8211−8241.
(47) Kubelka, P.; Munk, F. An Article on Optics of Paint Layers. *Z. Technol. Phys.* **1931**, *12* (1930), 593−601.
(48) Sheldrick, G. M. SHELXT − Integrated Space-Group and Crystal-Structure Determination. *Acta Crystallogr., Sect. A: Found. Adv.* **2015**, *71* (1), 3−8.
(49) Sheldrick, G. M. Crystal Structure Refinement with SHELXL. *Acta Crystallogr., Sect. C: Struct. Chem.* **2015**, *71* (1), 3−8.
(50) Müller, P. Practical Suggestions for Better Crystal Structures. *Crystallogr. Rev.* **2009**, *15* (1), 57−83.

https://doi.org/10.1021/jacs.1c09106
J. Am. Chem. Soc. 2021, 143, 20256−20263